Process Biochemistry 169 (2026) 214–225

Contents lists available at ScienceDirect

Process Biochemistry

journal homepage: www.elsevier.com/locate/procbio

Mechanistic insights into microwave-assisted ethyl acetate extraction of natural astaxanthin from *Paracoccus* sp. for functional products and cost estimation

Cassamo U. Mussagy [a,*], Angie V. Caicedo-Paz [a], Cristobál N. Alvarado-Holtheuer [a], M. Shaaban Sadek [b], Ahmad Mustafa [c], Diakaridia Sangaré [d]

[a] Laboratorio de Desarrollo de Bioprocesos Sostenibles (Labisost), Escuela de Agronomía, Facultad de Ciencias Agronómicas y de los Alimentos, Pontificia Universidad Católica de Valparaíso, Casilla 4-D, Quillota 2260000, Chile
[b] Department of Chemical Engineering , King Fahd University of Petroleum & Minerals (KFUPM), Dhahran, Saudi Arabia
[c] Faculty of Engineering, October University for Modern Sciences and Arts (MSA), Giza, Egypt
[d] CIRAD, UPR BioWooEB, 73 rue Jean-François Breton, Montpellier F-34398, France

ARTICLE INFO

Keywords:
Microwave-assisted extraction
Computational fluid dynamics modeling
Natural carotenoids
Green solvents
Techno-economic analysis

ABSTRACT

This study investigates a microwave-assisted extraction (MAE) process for the recovery of astaxanthin-rich extract (ARE) from *Paracoccus carotinifaciens* using ethyl acetate as a recyclable green solvent, integrating mechanistic modeling and techno-economic evaluation. Experimental data combined with computational fluid dynamics (CFD) revealed that microwave-induced thermal gradients and diffusion-driven mass transfer govern pigment release and recovery. Operating conditions (350–400 W; solid–liquid ratio ~1:30) yielded approximately 40 mg AXT eq./g within 40 min, while preventing thermal degradation. The kinetic model showed strong agreement with experimental data ($R^2 = 0.98$). The recovered ARE was successfully incorporated into a lip balm formulation, exhibiting uniform reddish–orange coloration and good stability. A preliminary techno-economic assessment indicated strong economic potential, with a return on investment (ROI) of 168% and a net present value (NPV) of $648.8 million, supporting the potential industrial scalability and economic feasibility of the proposed process. Overall, this work provides a framework combining process optimization, mechanistic understanding, and application potential for the sustainable recovery of microbial carotenoids.

1. Introduction

The cosmetic industry encompasses a broad spectrum of formulations, with the lip care segment, particularly lipsticks and glosses representing a dynamic area of innovation [1]. Advances in formulation science and increasing consumer awareness have prompted a pronounced shift toward natural and sustainable products enriched with bioactive compounds. This tendency aligns with the global expansion of the functional cosmetics market, which is projected to grow from USD 3.3 billion in 2022 to USD 4.6 billion by 2028, at a compound annual growth rate (CAGR) of 5.4% [2]. The increasing demand for multifunctional products that promote skin health, combined with heightened environmental awareness, continues to drive research and development in this sector. Within this context, natural pigments with biological activity have gained remarkable attention as multifunctional ingredients for next-generation cosmetic formulations. Among these bioactive compounds, astaxanthin (AXT) stands out as a potent colorant and antioxidant carotenoid with multiple biological properties, such as anti-inflammatory, photoprotective, and anti-aging effects [3–5]. Natural AXT, produced mainly by microalgae *Haematococcus pluvialis* [6–9] and bacteria *Paracoccus carotinifaciens* [10–12], has demonstrated superior antioxidant capacity and bioavailability compared to its synthetic AXT [13], making it particularly attractive for cosmetic applications. Besides its biological activity, AXT also provides intense coloration ranging from orange to deep red, making it ideal for use as a natural pigment in cosmetic formulations [14,15].

However, one of the main challenges in the industrial application of natural pigments lies in the cost-effective and sustainable recovery of intracellular biomolecules [16]. In many microorganisms, carotenoids such as AXT are biosynthesized and accumulated within the cells, which

* Corresponding author.
E-mail address: cassamo.mussagy@pucv.cl (C.U. Mussagy).

https://doi.org/10.1016/j.procbio.2026.08.007
Received 21 February 2026; Received in revised form 5 August 2026; Accepted 11 August 2026
Available online 13 August 2026

makes their recovery particularly demanding since the cell wall acts as a robust physical barrier that limits solvent penetration and pigment release [6,9,17,18]. Consequently, efficient extraction technologies capable of disrupting the cell wall and releasing the intracellular compounds are required, while simultaneously preserving their structural integrity and bioactivity. Conventional extraction procedures including Soxhlet and maceration often rely on toxic volatile organic compounds (VOCs), such as hexane, which pose significant environmental and safety concerns [19]. In contrast, green solvents such as ethyl acetate (EtOAc), a biodegradable solvent approved by the U.S. Food and Drug Administration (FDA) under additive and GRAS regulations (21 CFR Parts 170–186), are widely used in cosmetic formulations and have emerged as promising alternatives owing to their strong solvation capacity and high recyclability [20].

To further enhance extraction performance, various process intensification techniques to recovery AXT, including supercritical fluid extraction (SFE) [21–23], ultrasound-assisted extraction (UAE) [24–26], and microwave-assisted extraction (MAE) [27,28], have been explored. Among them, MAE has gained increasing attention due to its high extraction efficiency, shorter processing time, and reduced solvent consumption. Despite these advantages, the mechanistic understanding of MAE remains limited, as extraction performance is strongly influenced by several factors, including the type of biomolecule, solvent polarity, microwave power, and biomass characteristics [29,30]. Computational Fluid Dynamics (CFD) emerges as a powerful numerical tool to elucidate the coupled physical and chemical phenomena that govern MAE [27,31]. CFD allows prediction of the spatial distribution of the electromagnetic field and power absorption within the reactor, identifying potential "hot spots" and thermal gradients generated during microwave heating. When integrated with mass and energy transport models, CFD enables quantitative assessment of solvent dynamics, temperature evolution, and diffusion-driven AXT release [27]. In our previous work [27], CFD modeling was employed to simulate the electromagnetic field, heat transfer, and mass transport phenomena within a modified microwave reactor for the recovery of astaxanthin-rich extracts (ARE) from *Paracoccus carotinifaciens* using deep eutectic solvents (DES). That study revealed a detailed mechanistic understanding of how microwave irradiation interacts with solvent–bacterial biomass systems, elucidating the influence of dielectric properties, cavity geometry, and stirring conditions on energy absorption and solute diffusion. These insights laid the groundwork for the present investigation, which extends the application of MW-assisted extraction beyond recovery efficiency by employing green and recyclable solvents, while also exploring its potential integration into cosmetic formulations and techno-economic sustainability assessment.

Accordingly, this work aims to design, model, and evaluate a sustainable process for the recovery and application of *Paracoccus carotinifaciens*-derived ARE. This study goes beyond conventional extraction optimization by integrating mechanistic modeling (kinetics + CFD), green solvent-based MAE, functional product formulation, and techno-economic evaluation into a unified framework, providing new insights into microwave-driven extraction phenomena and bridging the gap between laboratory-scale recovery and industrial application. The study is structured into three main stages: *(i)* extraction and mechanistic modeling of the MAE bioprocess, combining kinetic parameter estimation and CFD simulations to elucidate the heat and mass transfer phenomena governing ARE release; *(ii)* formulation and characterization of a natural lip balm prototype incorporating the recovered MAE-ARE, with a focus on color uniformity, chromatic properties, and formulation stability; and *(iii)* TEA of the integrated process to assess its economic feasibility, identify key cost drivers, and establish sustainability indicators for potential industrial implementation.

2. Materials and methods

2.1. Raw material and chemicals

Lyophilized cells of the gram-negative marine bacterium *Paracoccus carotinifaciens* were kindly provided by the ENEOS Group (Tokyo, Japan). The all-E-astaxanthin standard was obtained from Sigma-Aldrich (St. Louis, MO, USA). Ethyl acetate (EtOAc, ≥99.5%) was used as a green biosolvent for the extraction of ARE. Natural beeswax (Materias Primas MMPP, Valparaíso, Chile), virgin coconut oil (B. Organics, Santiago, Chile), cocoa butter (Nativo Natural, Santiago, Chile), and vitamin E (Milagro del Bosque, Santiago, Chile) were purchased from certified cosmetic-grade suppliers. All reagents were of analytical or cosmetic grade and were used without further purification.

2.2. Extraction procedure

The solid–liquid extraction (SLE) of the ARE was conducted in a 250 mL spherical glass reactor containing 1 g of *P. carotinifaciens* biomass and 20, 30, or 40 mL of ethyl acetate (EtOAc). The extraction was performed using a commercial microwave (MW) system (Midea model MMP, Santiago de Chile, Chile) equipped with an external thermocouple and a magnetic stirrer to ensure homogeneous temperature distribution and prevent local overheating. The MW setup was previously calibrated and operated under the same configuration and parameters described in 2.3 (Numerical modeling approach). After extraction, the mixtures were centrifuged using an Orto Alresa Minicen centrifuge (Madrid, Spain) at 2500 ×g and 25 °C for 6 min. The resulting ARE-rich supernatants were carefully collected under minimal light exposure to prevent photooxidative degradation and stored in amber vials at 4 °C until further analysis. The astaxanthin content in the extracts was determined by UV–Vis spectrophotometry and expressed as astaxanthin equivalents [32]. Absorbance was measured at 474 nm using ethyl acetate as blank. A calibration curve was constructed using pure AXT standard, and the results were expressed as mg of AXT per liter (mg AXT/L). Considering that *P. carotinifaciens* biomass contains approximately 90% AXT and 10% other carotenoids, the measured values represent total carotenoids in the form of an astaxanthin-rich extract (ARE). The extraction yield was calculated and expressed as mg of ARE equivalents per g of dry biomass (mg ARE eq./g).

2.3. Numerical modeling approach

All experimental and simulation procedures were conducted following the same methodology described in our previous publication [27]. Briefly, the microwave configuration, operating at a fixed frequency of 2.45 GHz and an applied power of 400 W, as well as the geometric setup, material properties, and boundary conditions of the CFD model, were identical to those previously validated. The electromagnetic field, heat transfer, and mass transport were solved in COMSOL Multiphysics using Maxwell's equations, the energy balance for porous media, and Fick's second law for diffusive transport. Microwave energy absorption was introduced as a volumetric heat source derived from electromagnetic power dissipation, allowing direct coupling between the electromagnetic field and the thermal response of the system. The resulting temperature gradients influence solvent properties and enhance mass transfer, which is represented through the coupled diffusion process in the liquid phase. The only modification introduced concerns the biomass-to-solvent ratio, which was systematically varied to investigate its influence on the extraction kinetics of ARE. The kinetic determination was conducted following the same procedure previously described in our recent publications [27], with a specific modification

introduced in the kinetic section to ensure consistency across extraction systems with different solvent volumes. The methodology is based on the pseudo-second-order (PSO) kinetic model, which has been extensively applied for SLE and sorption phenomena [33,34]. The PSO model was selected due to its suitability for describing solid–liquid extraction systems in which both diffusion and interfacial phenomena contribute to the overall mass transfer process, providing a consistent representation of the extraction kinetics under the present conditions. In the present work, the PSO formulation was expressed as:

$$\frac{d_Y}{dt} = \mathbf{k_i}\cdot(\mathbf{Y_{eq,i}} - \mathbf{Y})^2 \quad (1)$$

Where Y is the ARE yields in the liquid phase (mg extract per g of biomass), $Y_{eq,i}$ (mg/g) is the equilibrium yield for system i, calculated from the total extractable mass, and k_i (g/s·mg) is the apparent kinetic constant. The analytical integration of **Equation (1)** is given by the following expression:

$$\frac{\mathbf{1}}{(\mathbf{Y_{eq}} - \mathbf{Y})} = \frac{\mathbf{1}}{\boldsymbol{Y_{eq}} - \boldsymbol{Y_0}} + \mathbf{k_i t} \quad (2)$$

where Y_0 is the initial yield (t = 0) in the liquid phase. **Equation (1)** was used to determine the kinetic parameters by linear regression of $1/(Y_{eq,i}-Y)$ versus time, with the intercept fixed at $1/(Y_{eq,i}-Y_0)$.

For each extraction system (1 g of biomass in 20, 30, and 40 mL of solvent), the equilibrium concentrations $Y_{eq,i}$ were computed from the total recovery of ARE (52.47 mg/g) and the molecular weight of AXT (596.84 g/ mol), yielding fixed values derived by mass balance. The experimental yields–time data were then linearly regressed according to Equation **(2)** to determine the apparent constants k_i, and to assess the fit quality through the coefficient of determination (R^2). Since the reaction involves the same solute (AXT) under identical thermal and mechanical conditions, a unified intrinsic kinetic constant (k) common to all systems was assumed, while hydrodynamic and mass transfer effects were grouped into dimensionless diffusion efficiency factors. The relationship between apparent and intrinsic parameters is written in the Equation (**3**):

$$\mathbf{k_i} = \boldsymbol{k} \bullet \boldsymbol{\phi}\mathbf{i} \quad (3)$$

Each factor ϕ_i thus represents the combined influence of external film resistance and effective interfacial area per unit suspension volume. Substituting Equation (**3**) into Equation **(2)** yields the general model used for simulation and validation:

$$\mathbf{Y(t)} = \boldsymbol{Y_{eq,i}} - \frac{\mathbf{1}}{\boldsymbol{k} \bullet \boldsymbol{\phi_i} \bullet \mathbf{t} + \frac{1}{\boldsymbol{Y_{eq,i}} - \boldsymbol{Y_0}}} \quad (4)$$

This adaptation enables the evaluation of the kinetic response as a function of solvent volume, keeping the intrinsic reaction constant unchanged. The approach maintains full comparability with the previously validated CFD–kinetic framework and ensures that observed variations in extraction rate can be attributed solely to changes in the hydrodynamic and diffusive regimes imposed by the different biomass-to-solvent ratios. Note that, the concentration fields obtained from the CFD simulations represent numerical variables used to describe the transport and distribution of the target compound within the extraction domain. These simulated concentrations are intended to analyze mass-transfer behavior and extraction dynamics.

2.4. Lip balm formulation and chromatic analysis

The lip balm formulation was designed to evaluate the applicability of *P. carotinifaciens*-derived ARE as a natural pigment and antioxidant. The formulation was prepared at two scales: a laboratory batch (100 g) and a pilot market simulation unit (5 g). The base matrix consisted of natural beeswax (25%), virgin coconut oil (25%), cocoa butter (48.5%), and vitamin E (1.43%). The bacterial ARE was incorporated at 0.0035 g per 100 g of product (0.0035% w/w). The ARE was obtained through MAE using EtOAc following the procedure previous described. For each 100 g of lip balm, 1 g of *Paracoccus* biomass and 40 mL of EtOAc were used, followed by 80% solvent recovery after extraction. All components were melted in a thermostatic bath at 70 ± 2 °C under gentle stirring until complete homogenization. The ARE and vitamin E were added during cooling (below 45 °C) to prevent pigment degradation. The mixture was poured into 5 g lip balm containers and stored at 25 °C until further characterization. Color measurements were performed using a LS173 colorimeter (Shenzhen, China) operating under standard conditions with D65 illumination and a 10° standard observer according to the CIE 2015 10°. Chromatic coordinates (x_n, y_n) were determined, and visual appearance and pigment dispersion were also evaluated by visual inspection after four weeks of storage.

2.5. Techno-economic analysis framework

To model the production process of the lip balm formulated with *Paracoccus carotinifaciens* ARE, a process simulation was developed using Aspen Plus (AspenTech, USA). The objective of this simulation was to perform comprehensive material and energy balance analyses to evaluate process performance and understand the overall mass and energy flows throughout the system [35].

2.5.1. Economic assessment

The economic assessment of a process is as essential as its technological design when planning industrial-scale production. Techno-economic analysis (TEA) provides a structured framework to evaluate whether a process is economically viable. In this study, the TEA considered three key components: (i) potential revenues, (ii) capital and operational costs associated with process implementation and handling, and (iii) overall profitability indicators [36–38]. The objective of this comparison was to generate actionable insights to support stakeholders in evaluating the investment attractiveness of lip balm production based on *Paracoccus carotinifaciens* ARE.

2.5.2. Total capital investment

The fixed capital cost (FCC) encompasses expenditures associated with establishing the physical infrastructure of the process, including facility construction, equipment purchases and installation, and overall system design. Accounting for these costs at early project stages is critical to prevent delays and ensure realistic investment planning. FCC typically includes Inside Battery Limits (ISBL) and Outside Battery Limits (OSBL) costs, as well as engineering, procurement, construction (EPC) services and contingency allowances [36]. Estimating ISBL expenses is a key part of determining whether a project makes financial sense. One common approach is the Bridgewater method [39], which is especially helpful when detailed design data is limited, something often true in early-stage process development. The estimation method is based on three primary design inputs: the plant capacity (expressed as annual production in metric tons), the fractional process conversion, and the number of major processing stages. The latter includes core operational units (e.g., reactors and separators) but excludes auxiliary equipment such as pumps and heat exchangers. In the present study, the plant capacity was defined as 396 t $year^{-1}$, with an overall conversion efficiency of 7%, and a total of seven main functional units. Since the production scale is below 60,000 t $year^{-1}$, the fixed capital cost was calculated using the Bridgewater equation, which is appropriate for small- to medium-scale industrial facilities:

$$C = 380,000 \quad N\left(\frac{Q}{S}\right)^{0.3} \quad (5)$$

Where C is the inside battery limit costs (US $), N denotes number of functional units, Q refers to plant capacity (tons per year), and S is fractional conversion.

Outside battery limit (OSBL) costs include all infrastructure and services located outside the core processing units but necessary for plant operation. These components typically cover storage facilities for raw materials and final products, utility supply systems (e.g., water, electricity, steam), and waste treatment installations, as well as any required off-site infrastructure upgrades. In industrial practice, when detailed site-specific data are unavailable, OSBL costs are commonly estimated as a percentage of the inside battery limit (ISBL) cost. Reported values range from 10% to 100% of ISBL, depending on project scale and site complexity [36]. In this study, OSBL costs were assumed to be 30% of the ISBL cost, with the understanding that this estimate may be refined as more detailed site information becomes available in future project stages. Engineering costs (EC) refer to the design and construction activities associated with the technological aspects of the facility. These include the work of chemical, mechanical, and process engineers responsible for equipment selection, plant layout, and control system design. At the preliminary stage, these costs cannot be determined precisely, as they largely depend on the scope of the project and prevailing economic conditions. In large-scale industrial projects, EC is typically estimated as a percentage of the total direct capital cost (i.e., ISBL + OSBL). For this preliminary assessment, an average value of 15% was adopted to establish a reasonable baseline. This assumption can be refined in subsequent design stages as more detailed engineering requirements become available.

Contingency costs are included in the project budget to account for unforeseen events that may affect the overall expenditure. These contingencies may arise from fluctuations in material prices, delays in equipment delivery, or engineering-related construction issues. Typically, contingency is estimated at around 10% of the direct capital cost (ISBL + OSBL), depending on the level of process or technological uncertainty. In the present study, a value of 15% was adopted to provide a conservative safety margin, reflecting the use of well-established and low-risk technologies while maintaining realistic cost projections. For the present analysis, the working capital was assumed to be 15% of the total direct capital cost (ISBL + OSBL), which represents an industry-standard benchmark. This percentage provides a reasonable initial estimate for evaluating day-to-day operational expenses during plant operation. As more detailed design and cost data become available, this assumption can be refined to improve the accuracy of the financial projections.

Start-up cost includes the one-time initial amount needed for the start-up for the initiation of the commencement of the plant, the staff trainings for the safety features and the handling, the first checking for the quality of the product, and the regulatory license such as the environmental authorization and waste discharge authorization. Additionally, consumables (e.g., catalysts and solvents) and utilities (e.g., electricity and water) for the commissioning also form the part of the initial amount. In this initial step, we presumed the 15% conservative rate for the start-up cost for the entire direct capital cost (ISBL + OSBL), an industry average facility size match. During the life of the project, it shall be more precisely matched based on the detailed commissioning schedule, the requirements for the vendors, and the ramp-up plan for the operable accuracy for budgeting [40].

2.5.3. Operating expenditure (OPEX)

Operating costs refer to the recurring expenses required to maintain the continuous operation of the production facility. These costs directly influence the day-to-day functioning of the plant and have an immediate impact on the profitability of the project. The fixed cost of production (FCOP) represents the portion of operating costs that remains constant within the plant's designed production capacity. Because these expenses do not vary with throughput, they are critical in assessing the economic feasibility of the process, and their reduction is generally difficult once the facility is operational. Labor costs constitute a major component of the FCOP and include wages and salaries for trained personnel, such as operators and supervisors required for routine operations. The number of staff required per shift strongly affects the total labor expenditure. Table S1 from ESI summarizes the variables considered in calculating the FCOP, along with the corresponding assumptions applied in the computational procedure. A clear understanding of the FCOP is therefore essential when evaluating project feasibility and developing strategies for managing recurring operational expenses [36,41].

Variable Cost of Production (VCOP) is associated with the production volume of the plant and involves the cost for utilities, raw materials, consumables, product packaging and movement, and waste removal. With more design and operating detail, the accuracy in the estimate for VCOP becomes more precise. Whereas with FCOP no scope exists for any cost optimization with design or operating improvement, VCOP offers scope for cost optimization with design or operating improvement, for which an ongoing effort for any cost reduction is inevitable. The principal revenue source for the project arises from the sale of the lip balms produced, representing the final commercial product of the process and the basis for evaluating economic return. One of the most important comparison measures is the gross margin, and this is the realized revenue for the entire project minus the cost for the raw materials. This is computed using the following equation:

$$Gross\ Margin = Revenues - Raw\ Material\ Cost \quad (6)$$

This is the amount that is left with sales revenue when the direct cost for raw materials is deducted. The larger the gross margin is, the more the project is profitable since the more amount is left for other operating costs for becoming profitable.

2.5.4. Profitability analysis

Profit analysis is a key component of project evaluation, as it reflects the capacity of the process to generate financial returns. Net profit is particularly relevant, as it represents the remaining earnings after all operating expenses, depreciation, and other costs have been deducted. The Cash Cost of Production (CCOP) is also a critical indicator of process feasibility, as it quantifies the actual cash expenditure required to produce the lip balm, excluding the cost of invested equity capital. The CCOP was calculated using the following expression:

$$CCOP = VCOP + FCOP - ByProduct\ Revenue \quad (7)$$

The project's gross profit is obtained by deducting the CCOP from the income earned from the sale of lip balms. This is the profit before taxes are considered. The net profit, the last measure of profitability, which considers all the costs, including taxes. The net profit can be expressed as:

$$Net\ Profit = Gross\ Profit - Tax\ Expense \quad (8)$$

Where the tax expense is calculated as:

$$Tax\,Expense = Taxable\,Income\ (Gross\,Profit - Depreciation)\ x\,Tax\,Rate \quad (9)$$

The applicable tax rate must be determined in accordance with relevant tax legislation and accounting standards. Depreciation is a commonly applied tax deduction and is subtracted from gross profit to obtain taxable income. Corporate income tax is levied on net earnings, and the specific rate depends on jurisdiction, industrial sector, and current regulatory frameworks. For reference, the federal corporate tax rate in the United States was 21% in 2018 [42]. Depreciation represents the systematic allocation of an asset's cost over its useful life. It reduces the book value of capital assets and provides a tax benefit by lowering taxable income. For the purpose of this cost estimation, a 5-year recovery period was assumed, with depreciation charges incorporated into the project cash flow. The choice of depreciation method and asset life may vary depending on local accounting practices and tax regulations. For financial appraisal, a discount rate of 11% was applied to account for the time value of money. This value reflects the minimum acceptable rate of return required for the project to be considered economically viable.

2.5.5. Financial performance indicators

This section outlines the key financial indicators used to evaluate the economic feasibility of the project. These indicators incorporate the time value of money, acknowledging that a dollar received today has greater value than a dollar received in the future. The net present value (NPV) represents the difference between the present values of project cash inflows and outflows. It is calculated as:

$$NPV = \sum_{n=1}^{n=t} \frac{CF_n}{(1+i)^n} \quad (10)$$

Where *CFn* is cash flow in each particular year, where *t* is the project life in years, and *i* denotes the discount rate. A positive NPV indicates that the project is expected to generate value in excess of its cost.

Return on investment (ROI) measures the profitability of the project relative to the initial capital expenditure (a higher ROI indicates a more favorable investment) and is calculated as:

$$ROI = \frac{Average\ Annual\ Profit}{Initial\ investment} \times 100 \quad (11)$$

The internal rate of return (IRR) is the discount rate that results in an NPV of zero. It represents the minimum acceptable rate of return for the project, accounting for the time value of money [36]. The IRR is determined by solving:

$$IRR = \sum_{n=1}^{n=t} \frac{CF_n}{(1+i)^n} = 0 \quad (12)$$

The payback period is the time required to recover the initial investment. It provides a simple measure of project liquidity and investment risk [36]. It is calculated as:

$$Payback\ Period = \frac{Total\ Investment}{Average\ Annual\ Cash\ Flow} \quad (13)$$

Note that, a shorter payback period indicates lower financial risk, as the initial investment is recovered sooner.

2.6. Statistical analysis

All extraction experiments were performed in triplicate, and the results are presented as mean ± standard deviation. Note that, statistical analyses were performed using GraphPad Prism 9. Differences between experimental conditions were evaluated by one-way analysis of variance (ANOVA), followed by Tukey's post hoc test for multiple comparisons. A significance level of $p < 0.05$ was considered statistically significant. Kinetic parameters were determined by linear regression using the pseudo-second-order model. The goodness of fit was assessed by the coefficient of determination (R^2) and root mean square error (RMSE), providing a quantitative evaluation of model accuracy.

3. Results and discussion

3.1. Mechanistic understanding of extraction through kinetic modeling and CFD

To gain a mechanistic understanding of the factors governing ARE release from the biomass matrix, the extraction performance was quantified experimentally and interpreted through a kinetic modeling framework, whereas CFD simulations were employed to resolve the local heat and mass transfer phenomena occurring during MAE. In this context, the integration of kinetic parameter estimation with CFD enables a direct analysis of how microwave energy deposition affects temperature distribution and mass transfer within the reactor. The combined experimental and numerical approach therefore provides a mechanistic interpretation of the extraction process under the studied operating conditions.

3.1.1. Estimation of pseudo-second-order kinetic parameters

The kinetic constant k was individually determined for each extraction system (1 g / 20, 30, and 40 mL) by fitting the pseudo-second-order model to the experimental yield data according to **Equation (3).** The corresponding coefficients of determination were $R^2 = 0.987$, 0.979, and 0.954, respectively, confirming the suitability of the pseudo-second-order kinetics to represent the extraction process, particularly under microwave-assisted conditions where both diffusion and external film transfer contribute to the overall rate [43]. The high linearity observed in Fig. 1 indicates that the pseudo-second-order formulation provides a good description of the experimental data throughout the extraction period. The initial yield ($Y_0 = 7.55 \pm 1.02$ mg/g) was considered constant for all experiments, corresponding to the mean of the initial experimental points. The kinetic constants obtained —$k_{20} = 5.98 \times 10^{-3}$, $k_{30} = 5.67 \times 10^{-3}$, and $k_{40} = 7.47 \times 10^{-4}$ [g/mg·min]—show a marked dependence on the solvent volume. This trend reveals that increasing solvent volume reduces the external mass-transfer resistance and enhances solute diffusion toward the bulk phase, consistent with observations reported for other solid-liquid and plant-based extraction systems [44,45].

Similarly, the equilibrium yields estimated by the model ($Y_{eq,20}$=41.2, $Y_{eq,30}$=100.1 and $Y_{eq,40}$=109.0 mg/g of biomass) increase proportionally with the solvent volume, as expected from the higher solubility and reduced saturation effects at lower biomass-to-solvent ratios [44–46]. Consistently, within the studied range, the volume (V)–equilibrium relationship can be expressed as: $Y_{eq} = 3.39V - 18.27$ (mg/g). Fig. 1 shows that the slopes of the linearized relationships (corresponding to K_i) vary significantly with the extraction biomass-to-solvent ratio, emphasizing the dominant role of hydrodynamic conditions in determining the apparent rate constants. The pseudo-second-order model thus effectively captures both the kinetic and diffusive aspects of the SLE process, offering a physically consistent representation of the system behavior under varying solvent volumes. Furthermore, to preserve a single intrinsic constant across systems, the apparent rate constants were recast in **Equation (3)**, where $k = 1.36 \times 10^{-3}$ g/ mg.min is the unified intrinsic kinetic constant, and ϕi is a dimensionless efficiency factor representing hydrodynamic and diffusive effects. The diffusive–hydrodynamic factor showed a linear dependence on the biomass-to-solvent ratio, expressed as $\phi i = 165.66$ (B/S) – 4.20 (with R^2=0.87), confirming that the overall mass-transfer efficiency decreases with increasing solid loading. All determined parameters—including Y_0, Y_{eq}, k_i, ϕ_i and R^2 are summarized in Table 1.

Recent studies on ARE recovery from *P. carotinifaciens* have explored alternative intensification strategies. For instance, ultrasound-assisted extraction using deep eutectic solvents (DES) has been reported to achieve high recovery efficiencies within short processing times (~8 min), mainly attributed to cavitation-enhanced mass transfer. Similarly, bio-based solvent systems, such as ethyl acetate–acetic acid mixtures, have demonstrated extraction capacities of up to 3.28 mg/mL under optimized conditions (78 °C, 10 min), with further improvements achieved through ultrasound assistance [32,47]. Although direct comparison is limited due to differences in reported units, extraction systems, and operating conditions, as well as variability in carotenoid content across *P. carotinifaciens* production batches, the present MAE-based approach achieved a maximum yield of approximately 40 mg AXT eq./g within 40 min under controlled conditions.

3.1.2. Validation of model with CFD simulation

3.1.2.1. CFD simulation of microwave-assisted extraction. The CFD simulation was employed to capture the spatio-temporal evolution of temperature and concentration gradients inside the extraction reactor during the microwave heating. The kinetic parameters determined experimentally (Table 1) were integrated into a coupled electromagnetic–thermal–mass-transfer model of the stirred reactor to

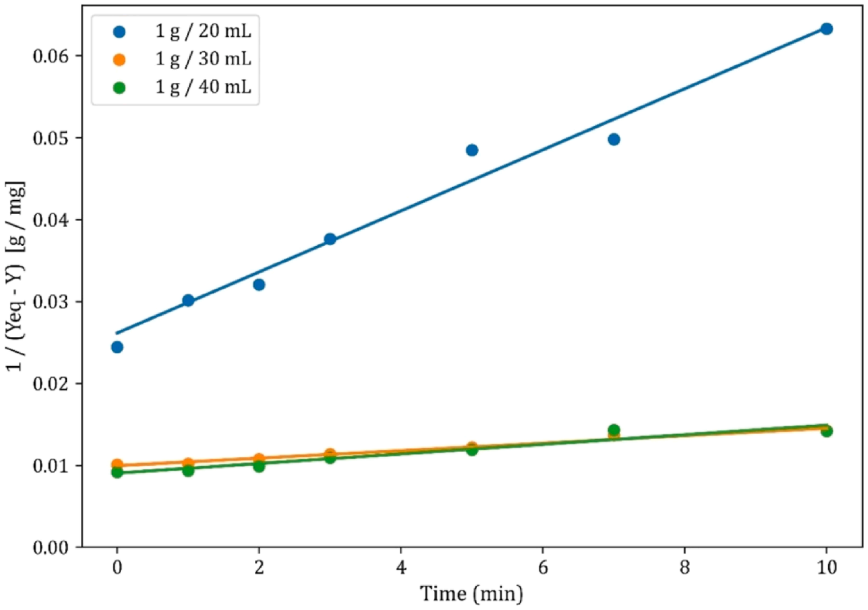

Fig. 1. Linearization of the pseudo-second-order kinetic model for different biomass-to-solvent ratios.

Table 1
Kinetics parameters obtained from the pseudo-second-order model.

Mixture	$Y_{eq,i}$ (mg/g)	ki (g/mg.min)	ϕ_i (–)	R^2
1:20	41.2	5.98×10^{-3}	4.387	0.987
1:30	100.1	5.67×10^{-3}	0.416	0.979
1:40	109.0	0.747×10^{-3}	0.548	0.954

resolve the dynamic extraction of astaxanthin-rich compounds under realistic operating conditions. The simulation was performed by coupling frequency-domain Maxwell's equations for the electromagnetic field with the transient energy balance in the liquid phase and convection–diffusion transport for the solute. Microwave absorption was represented by heat source of 400 W within 10 min of irradiation, while mixing at 300 rpm was imposed to emulate the stirred-reactor hydrodynamics and promote near-uniform bulk convection.

Fig. 2 shows the simulated temperature and ARE yield fields inside the microwave-assisted stirred reactor at 0, 2, 5, and 10 min, for a biomass-to-solvent ratio of 1 g per 30 mL. Fig. 2 **(a–d)** shows the temperature evolution inside the reactor. Due to continuous stirring (300 rpm), convective mixing promotes rapid homogenization of the liquid phase, resulting in nearly uniform temperature profiles during heating. No macroscopic "*hot spots*" are observed within the bulk domain, although slightly lower temperatures are detected near the reactor wall due to boundary heat losses. Fig. 2 **(e–h)** presents the simulated solute yield distribution. Similar to the temperature field, stirring induces rapid spatial homogenization of the extracted astaxanthin within the liquid phase. While the earliest simulation time reflects the onset of solute release at the biomass–solvent interface,

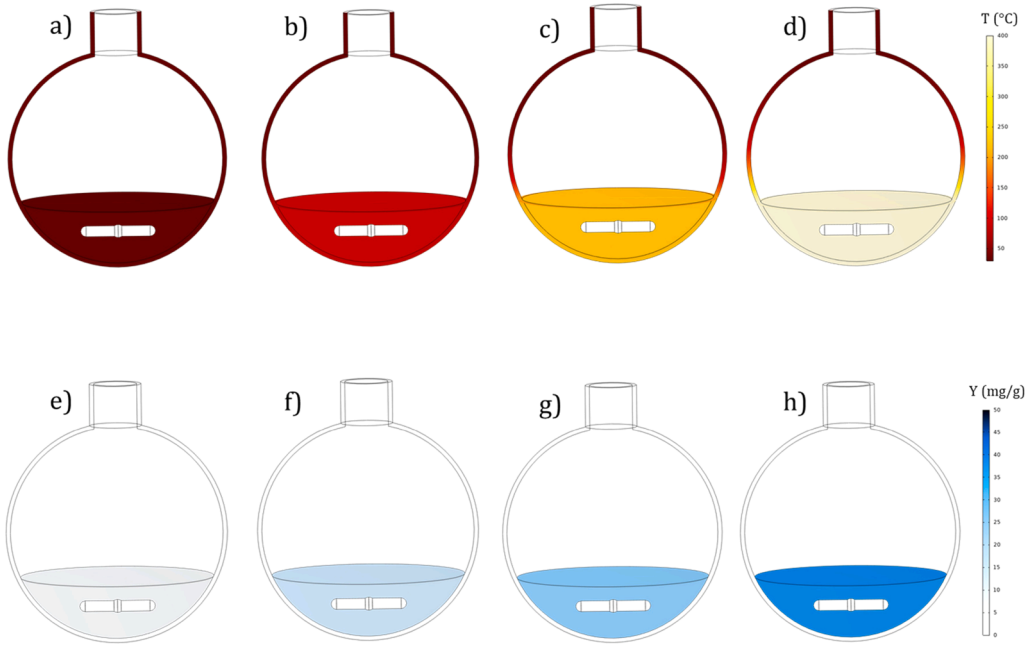

Fig. 2. Simulated temperature (a–d) and ARE yield (e–h) distributions inside the microwave-assisted stirred reactor at different heating times (0, 2, 5, and 10 min).

convective transport quickly equalizes concentration gradients across the reactor volume. At the start, the ARE yield is low (≈7.03 mg/g) and concentrated near the biomass–solvent interface. As heating progresses, increased molecular diffusion and reduced solvent viscosity accelerate solute dispersion, producing progressively more homogeneous yield fields throughout the reactor. Between 5 and 10 min, no substantial changes in ARE recovery are observed, indicating that the system is approaching extraction equilibrium. These numerical results corroborate the physical consistency of the coupled electromagnetic–thermal–mass-transfer model and support the experimentally determined kinetic parameters. Note that, the initial yield (Y_0) value reflects the presence of a readily extractable astaxanthin fraction originating from partially disrupted cells during upstream biomass processing (harvesting, lyophilization, and handling), which becomes immediately solubilized upon solvent contact.

Although the CFD model successfully reproduced the experimental extraction trends and predicted relatively uniform temperature fields under stirred conditions, several simplifying assumptions should be acknowledged. The simulations assume effective bulk homogenization promoted by continuous stirring and therefore primarily describe reactor-scale behavior. Consequently, potential microscale temperature heterogeneities and localized microwave-induced heating near biomass particles are not explicitly resolved. Furthermore, mass transfer was represented through coupled convection–diffusion transport and experimentally derived kinetic parameters, whereas complex intraparticle diffusion phenomena and local structural variations within the biomass were not modeled separately. Therefore, the present framework should be interpreted as a mechanistic approximation of the dominant electromagnetic, thermal, and mass-transfer processes rather than a complete description of all microscopic transport phenomena occurring during microwave-assisted extraction.

3.1.2.2. CFD validation of the kinetic model. Fig. 3 compares the experimental data with the numerical predictions expressed as extraction yields (mg extract per g biomass). The model accurately reproduces the overall extraction profiles for all biomass-to-solvent ratios, showing an excellent quantitative agreement in the 1 g / 20 mL and 1 g / 30 mL systems, and a satisfactory representation for the 1 g / 40 mL case. The extraction behavior was analyzed using the pseudo-second-order kinetic model. The RMSE values (0.94, 1.57, and 3.24 mg/g) and determination coefficients (R^2 = 0.987, 0.979, and 0.954, respectively) confirm the robustness of the pseudo-second-order model to describe the dynamic extraction behavior under microwave-assisted conditions.

The shape of the simulated curves closely follows the experimental trends, indicating that the kinetic constants and equilibrium yields estimated through the nonlinear regression effectively capture the dominant mass-transfer phenomena. For the higher solvent volume (1 g / 40 mL), a slight deviation appears at longer extraction times, where the model slightly overpredicts the extraction rate.

This deviation likely originates from the prolonged persistence of the driving concentration difference ($(Y_{eq}-Y_f)$ and the resulting transition from film-controlled to mixed external–internal diffusion regimes. This behavior contributes to the nonlinear shape of the extraction curves, as the progressive decrease in the driving force (Yeq − Y) and the transition from external mass transfer to intraparticle diffusion modify the extraction rate over time. The observed trend is consistent with a regime transition: while the pseudo-second-order model captures the overall kinetics of ARE extraction, the systematic underprediction at large solvent volumes can be rationalized by an enhanced intraparticle-diffusion contribution. This implies a progressive shift from film-boundary control to intraparticle-diffusion control, a regime that is only partially represented by the current single-step model framework [48,49]. For extended extraction time or increased solvent, an expanded model incorporating an effective diffusion term could further refine the description of internal transport resistance. Although there are slight deviations from the 1/40 biomass-solvent ratio, the model captures the overall behavior of the process and provides a physically consistent basis for further computational exploration. In particular, the validated framework can now be used to perform a sensitivity analysis aimed at identifying the effects of operational variables, such as microwave power, solvent volume, and stirring speed, on the coupled electromagnetic, thermal, and mass transfer phenomena.

3.1.3. Sensitivity analysis

Fig. 4 shows a surface describing the expected extraction yield of ARE as a function of microwave power (200–600 W) and the biomass-to-solvent ratio (1:50–1:10). The contour map reveals a nonlinear coupling between the two variables, reflecting the opposing effects of the electromagnetic energy input and solvent-mediated diffusion on the overall extraction yield. The white markers represent the experimental data points overlaid on the simulated surface to show the agreement between numerical predictions and experimental results.

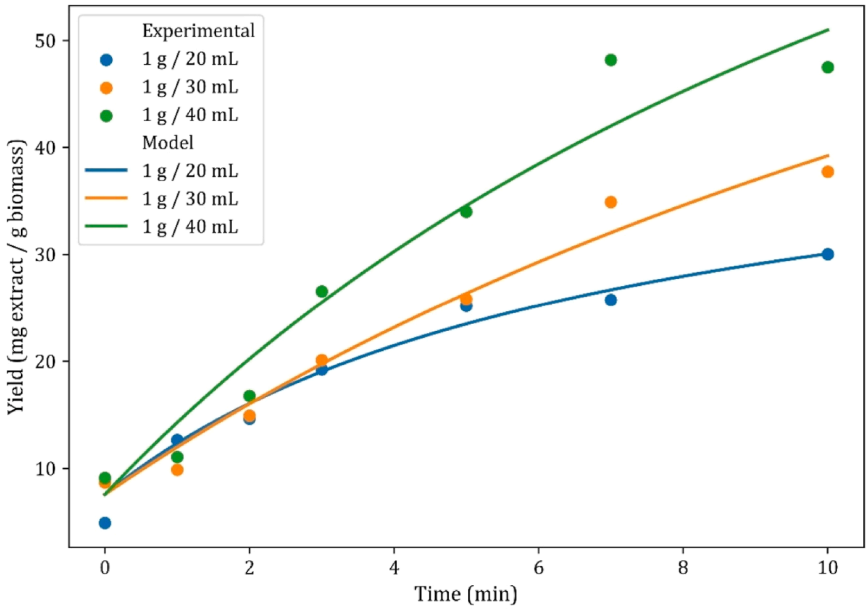

Fig. 3. Evolution of experimental data and model simulated results ARE rich extract recovery.

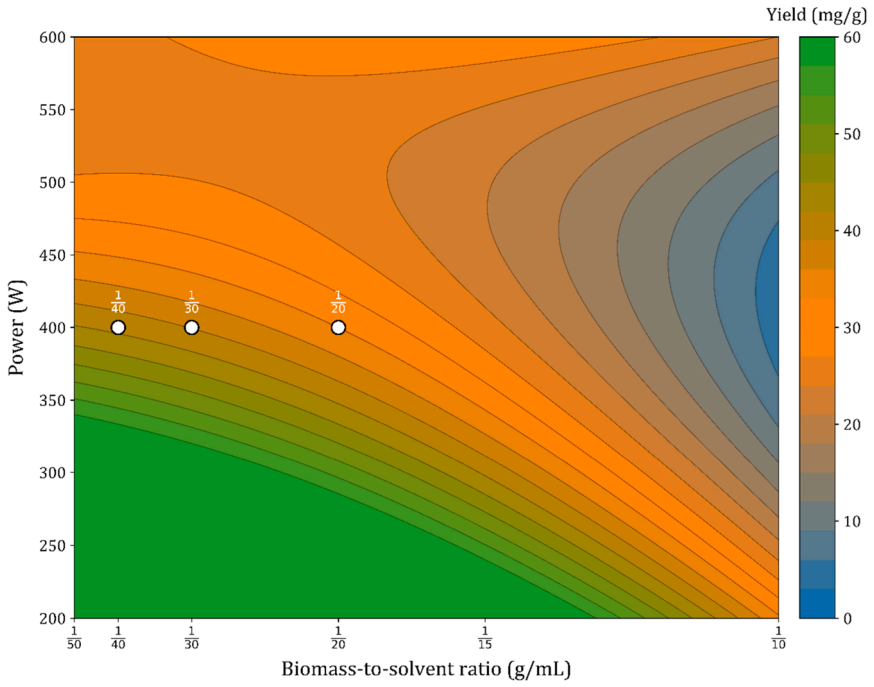

Fig. 4. Contour map showing the effect of microwave power and biomass-to-solvent ratio on predicted extraction yield during microwave-assisted extraction of ARE.

At low biomass-to-solvent ratios (1:50–1:30), which correspond to greater solvent availability, extraction yields remain high across a wide range of microwave powers. This region (lower left of the map) represents a regime dominated by mass transfer, in which the external resistance of the film is minimal. The system shows yields close to saturation even at moderate power levels (250–350 W), indicating that diffusion and solubilization are not limited by thermal gradients under these conditions. Similar behaviors have been described in MAE of carotenoids and polyphenols, where a lower biomass-solvent ratio increases the effective interfacial area and reduces diffusion limitations due to viscosity [50]. In contrast, as the biomass fraction increases (ratios approaching 1:10), the extraction yield decreases markedly even at elevated microwave powers. This shift indicates a transition toward a solid-loading-controlled regime, dominated by intraparticle diffusion and local heating heterogeneities. The reduction of solvent volume limits molecular mobility and increases the effective viscosity, diminishing both convective turnover and solute solubility. The contour lines in the upper-right region of the figure become densely packed, illustrating a diminishing sensitivity to further power increments beyond 450 W. This plateau reflects the onset of thermal saturation, where additional power no longer translates into higher extraction efficiency due to constrained mass transport within the particle matrix. Between these extremes, a better operating range is observed around 350–400 W and B/S ≈ 1:30, where electromagnetic heating, diffusion, and hydrodynamic mixing are balanced. These conditions favor greater ARE recovery. From a process standpoint, moderate microwave power and a relatively low biomass load provide the best balance between energy consumption, extraction time, and thermal uniformity. However, these conditions require larger volumes of solvent, which increases heating time and solvent recovery costs.

3.2. Lip balm formulation and chromatic characterization

Most studies on microbial carotenoids focus primarily on optimizing extraction yield and pigment recovery, often overlooking the practical application and functional performance of the obtained extracts. In contrast, the present work advances beyond the extraction step by formulating a cosmetic prototype and performing an integrated economic evaluation to assess its feasibility and sustainability. Among the various formulations tested, the composition described in 2.4 provided the best visual uniformity, thus being selected for detailed analysis. As depicted in Fig. 5, the incorporation of *Paracoccus*-derived ARE extract imparted a visually uniform reddish–orange coloration to the lip balm, indicating homogeneous pigment dispersion within the lipid phase. The lipophilic environment provided by the beeswax–cocoa butter blend promoted pigment stabilization by reducing oxygen diffusion and limiting photooxidative degradation (two degradation paths of ARE). The addition of vitamin E further enhanced oxidative protection, acting synergistically with ARE molecules to maintain color intensity and matrix stability over time. Furthermore, the low ARE input (0.0035% w/w in the final product) and high solvent recovery (80%) demonstrate the efficiency and sustainability of the extraction system. Likewise, adding even a small concentration of ARE is enough to maintain a desirable color, which contributes significantly to the overall effectiveness of the system.

The resulting product exhibited strong chromatic intensity, confirming the high coloring power of the *Paracoccus*-derived extract in lipidic media. It is worth noting that the final hue may vary slightly depending on the formulation and manufacturer preferences, ranging from orange to deep red tones. This natural color variability is characteristic of ARE and offers formulation flexibility according to the desired aesthetic profile of the cosmetic product. In this case, the formulation keeps all characteristics we define for a "natural lip balm" as: *smooth texture*, *consistent structure*, *remaining luminosity* and *no pigment precipitation* after four weeks of storage at 25 °C, indicating good compatibility between the extract and the lipid excipients (Fig. 5).

The chromatic properties of the formulation were analyzed using the CIE 2015 10° chromaticity diagram (Fig. 5). The measured chromatic coordinates (x_n = 0.409; y_n = 0.453) fall within the orange–reddish region of the visible spectrum, dominated by red and yellow components typical of carotenoid pigments. The enlarged inset in Fig. 5 shows the 1 u′v′ color tolerance ellipse, indicating minimal coordinate dispersion and confirming apropiate color uniformity. The visual image of the lip balm confirms the measured chromatic response, showing a stable hue typical of natural pigments. These results confirm that the ARE's optical stability is maintained under formulation conditions and that its color

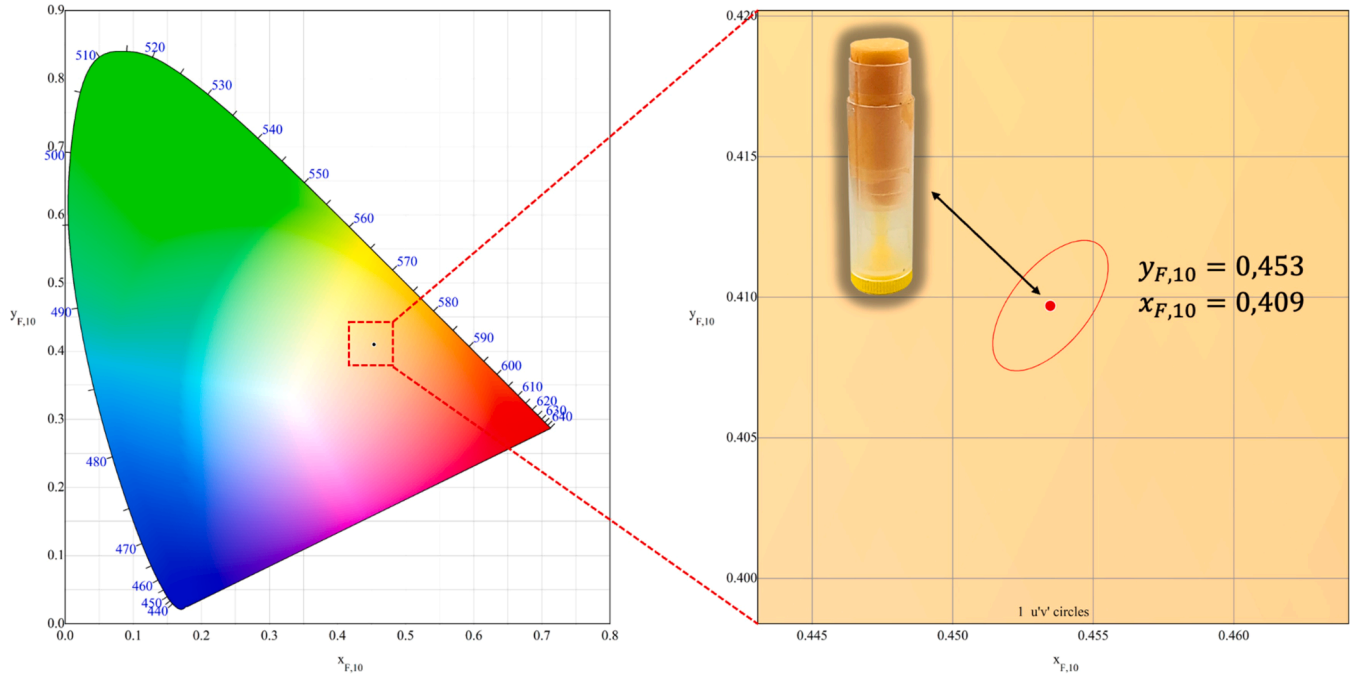

Fig. 5. CIE 2015 10° chromaticity diagram of the *Paracoccus*-based lip balm showing coordinates ($x_n = 0.409$; $y_n = 0.453$) in the orange–reddish region. The inset displays the product's visual appearance and color uniformity obtained with the *Paracoccus carotinifaciens* ARE.

properties can be precisely quantified by standard colorimetric analysis. The hue and stability obtained are characteristic of natural carotenoids, reinforcing the potential of *Paracoccus*-derived ARE as a sustainable and functional alternative to synthetic colorants in cosmetic formulations.

3.3. Techno-economic analysis

A comprehensive evaluation of economic sustainability is a critical component in the development of emerging bioprocesses. Beyond laboratory-scale optimization of MAE, extraction yield or product performance, it is essential to determine whether the proposed bioprocess can be translated into a cost-effective and industrially scalable operation. Accordingly, a techno-economic analysis (TEA) was performed to quantitatively assess the integrated system encompassing the MAE of *Paracoccus carotinifaciens*-derived ARE and its subsequent use in cosmetic formulation. This analysis provides an in-depth understanding of the relationship between process efficiency, solvent recovery, and product value, enabling the identification of key economic drivers and profitability indicators that define the economic feasibility and sustainability boundaries of the proposed microbial pigment production pathway. Capital expenditure represents a primary consideration for producers when initiating new ventures. The Inside Battery Limits (ISBL) cost constitutes a major component of this expenditure, as it encompasses the principal investment required for constructing the manufacturing facility. According to the Bridgewater method applied in this study, the estimated ISBL cost for the proposed process is approximately $35.54 million, as indicated in Table S2 from ESI. This amount reflects its huge proportion of overall capital spending. Aside from the capital outlay, the recurring costs of production are important for ascertaining the economic feasibility of the project. Table S3 from ESI and Fig. 6-A shows the itemized breakdown of the costs of the raw materials and products of the process. Moreover, Table S4 from ESI and Fig. 6-B shows a detailed breakdown of the total production expenses for lip balm manufacture, which equivalent to $137,710 per ton and 0.69 for each 5 g unit. This number is crucial to the project's overall financial assessment.

Comparing the current values of future cash inflows and outflows over a 15-year period, the Net current Value (NPV) analysis accounts for the time value of money. Strong economic feasibility for the project is shown by a positive NPV. The findings of the NPV analysis for the lip balm manufacturing process are shown in Table 2. The design phase, which entails the first financial expenditure, starts the project timetable in the first year. In the second year, construction and installation come next. It is anticipated that the facility would reach full production capacity by the third year. Despite this, the effects of depreciation are expected to cause gross profit to gradually decrease. The proposed method for the lip balm project has a positive net present value (NPV) of $648.8 million and a significant return on investment (ROI) of 168%, as shown in Table S4 from **ESI**. These numbers highlight the project's potential as a very lucrative investment opportunity. The IRR of the project stands at a notable 160%, which highlights the financial viability of the project. The payback period also stands at a mere 0.79 years, indicating fast recovery of the original capital investment. These findings and observations strongly speak for the economic viability and feasibility of the proposed process for the manufacture of lip balm. In conclusion, the economic analysis indicates a highly potential investment. Having a positive NPV, high ROI, favorable IRR, and relatively short payback period, this project is a sound financial project.

4. Conclusions

This study demonstrated the feasibility of recovering astaxanthin-rich extract (ARE) from *Paracoccus carotinifaciens* using microwave-assisted extraction (MAE) with ethyl acetate as a green solvent. The integration of kinetic modeling and CFD analysis provided insight into the heat and mass transfer mechanisms governing extraction, supporting process optimization. The process achieved efficient pigment recovery and was validated through a proof-of-concept cosmetic formulation. Techno-economic evaluation indicated strong economic potential (ROI = 168%; NPV = $648.8 million), supporting the potential scalability of the proposed system. However, this study is limited to laboratory-scale evaluation and proof-of-concept application. Future work should focus

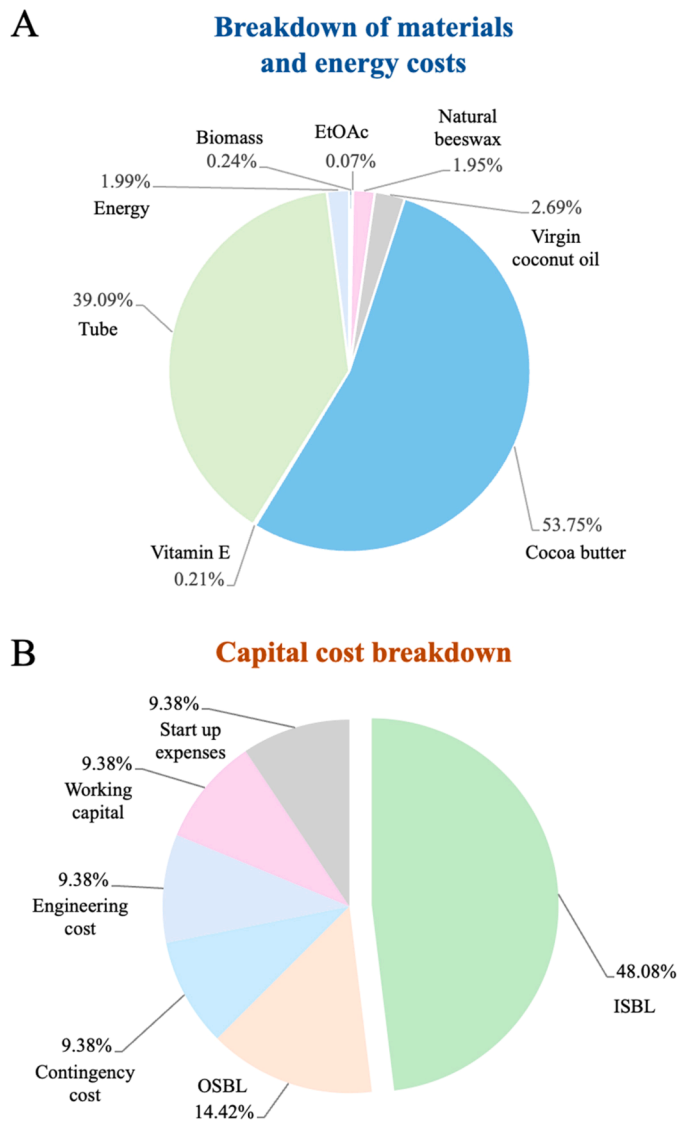

Fig. 6. A- Breakdown of materials and energy costs; (B) Capital cost breakdown. ISBL refers to Inside Battery Limits, and OSBL refers to Outside Battery Limits.

on process scale-up, optimization under industrially relevant conditions, and comprehensive evaluation of formulation performance, including physicochemical and sensory properties.

CRediT authorship contribution statement

M. Shaaban Sadek: Writing – original draft, Software, Methodology, Investigation. **Cristobál N. Alvarado-Holtheuer:** Software, Investigation. **Angie V. Caicedo-Paz:** Writing – review & editing, Writing – original draft, Investigation. **Mussagy Cassamo:** Writing – review & editing, Writing – original draft, Visualization, Validation, Supervision, Software, Resources, Project administration, Methodology, Investigation, Funding acquisition, Formal analysis, Data curation, Conceptualization. **Diakaridia Sangaré:** Writing – review & editing, Writing – original draft, Software, Investigation, Formal analysis, Conceptualization. **Ahmad Mustafa:** Writing – original draft, Supervision.

Funding

This research was supported by grants from National Research and

Table 2
Cash flow analysis for biomass conversion facility project.

Project life	Investment (%)	Capacity (%)	Depreciation	Investment	OPEX	Revenues	Gross Profit	Dep. Expenses	Taxable Income	Tax paid	Cash Flow	Dis. Cash Flow
0											0	0
1	0	0	0	0	$0.00	$0.00	$0.00	$0.00	$0.00	$0.00	$0.00	$0.00
2	100	0	0	$73,913,559	$0.00	$0.00	$0.00	$0.00	$0.00	$0.00	-$73,913,559	-$66,588,792
3	0	100	0.2		$54,533,365	$198,000,000	$143,466,634	$28,693,326	$114,773,307	$25,823,994	$117,642,639	$95,481,405
4	0	100	0.32		$54,533,365	$198,000,000	$143,466,634	$45,909,322	$97,557,311	$21,950,395	$121,516,239	$86,019,284
5	0	100	0.192		$54,533,365	$198,000,000	$143,466,634	$27,545,593	$115,921,040	$26,082,234	$117,384,399	$77,494,850
6	0	100	0.1152		$54,533,365	$198,000,000	$143,466,634	$16,527,356	$126,939,277	$28,561,337	$114,905,296	$69,815,180
7	0	100	0.1152		$54,533,365	$198,000,000	$143,466,634	$16,527,356	$126,939,277	$28,561,337	$114,905,296	$62,896,559
8	0	100	0.0576		$54,533,365	$198,000,000	$143,466,634	$8263,678	$135,202,955	$30,420,665	$113,045,968	$56,663,566
9	0	100	0		$54,533,365	$198,000,000	$143,466,634	$0.00	$143,466,634	$32,279,992	$111,186,641	$51,048,258
10	0	100	0		$54,533,365	$198,000,000	$143,466,634	$0.00	$143,466,634	$32,279,992	$111,186,641	$45,989,422
11	0	100	0		$54,533,365	$198,000,000	$143,466,634	$0.00	$143,466,634	$32,279,992	$111,186,641	$41,431,911
12	0	100	0		$54,533,365	$198,000,000	$143,466,634	$0.00	$143,466,634	$32,279,992	$111,186,641	$37,326,046
13	0	100	0		$54,533,365	$198,000,000	$143,466,634	$0.00	$143,466,634	$32,279,992	$111,186,641	$33,627,069
14	0	100	0		$54,533,365	$198,000,000	$143,466,634	$0.00	$143,466,634	$32,279,992	$111,186,641	$30,294,656
15	0	100	0		$54,533,365	$198,000,000	$143,466,634	$0.00	$143,466,634	$32,279,992	$111,186,641	$27,292,483
						ROI	**168%**				NPV	$648,791,904
						IRR	**160%**		Payback	**0.7898**	Years	

Development Agency - ANID: ANID/FONDECYT/1250170; ANID/FOVI/250065; ANID CTI250006; ANID-FAPESP/2025/18237-4.

Declaration of Competing Interest

There are no conflicts to declare.

Appendix A. Supporting information

Supplementary data associated with this article can be found in the online version at doi:10.1016/j.procbio.2026.08.007.

Data availability

Data will be made available on request.

References

[1] C. Heusèle, H. Cantin, F. Bonté, Lips and Lipsticks. in: Cosmetic Dermatology, Wiley, 2022, pp. 252–258, https://doi.org/10.1002/9781119676881.ch26.

[2] Markets and Markets, https://www.marketsandmarkets.com/Market-Reports/functional-cosmetics-market-208028292.html?gad_source=1&gad_campaignid=20828024545&gclid=Cj0KCQiA5abIBhCaARIsAM3-zFWH0P5Ej6E7U04D1e9omiJZTDnIFOjsWpykfxsrL958z9o6I7I1_tsaAmH8EALw_wcB, (2025). https://www.marketsandmarkets.com/Market-Reports/functional-cosmetics-market-208028292.html?gad_source=1&gad_campaignid=20828024545&gclid=Cj0KCQiA5abIBhCaARIsAM3-zFWH0P5Ej6E7U04D1e9omiJZTDnIFOjsWpykfxsrL958z9o6I7I1_tsaAmH8EALw_wcB (Accessed November 3, 2025).

[3] Y. Nishida, P. Berg, B. Shakersain, K. Hecht, A. Takikawa, R. Tao, Y. Kakuta, C. Uragami, H. Hashimoto, N. Misawa, T. Maoka, Astaxanthin: past, present, and future, Mar. Drugs 21 (2023) 514, https://doi.org/10.3390/md21100514.

[4] H. Hirakida, S. Nakamura, S. Inagaki, S. Tsuji, M. Hayashi, M. Shimazawa, H. Hara, Anti-diabetic effects of astaxanthin-rich extract derived from *Paracoccus carotinifaciens* on pancreatic β cells, J. Funct. Foods 97 (2022) 105252, https://doi.org/10.1016/j.jff.2022.105252.

[5] P.B. Demirel, B.G. Tuna, Anticancer properties of astaxanthin: a molecule of great promise. Global Perspectives on Astaxanthin, Elsevier, 2021, pp. 427–445, https://doi.org/10.1016/B978-0-12-823304-7.00003-9.

[6] X. Li, X. Wang, C. Duan, S. Yi, Z. Gao, C. Xiao, S.N. Agathos, G. Wang, J. Li, Biotechnological production of astaxanthin from the microalga *Haematococcus pluvialis*, Biotechnol. Adv. 43 (2020) 107602, https://doi.org/10.1016/j.biotechadv.2020.107602.

[7] K.S. Khoo, S.Y. Lee, C.W. Ooi, X. Fu, X. Miao, T.C. Ling, P.L. Show, Recent advances in biorefinery of astaxanthin from *Haematococcus pluvialis*, Bioresour. Technol. 288 (2019) 121606, https://doi.org/10.1016/j.biortech.2019.121606.

[8] R.T. Lorenz, G.R. Cysewski, Commercial potential for *Haematococcus* microalgae as a natural source of astaxanthin, Trends Biotechnol. 18 (2000) 160–167, https://doi.org/10.1016/S0167-7799(00)01433-5.

[9] I. Niizawa, B.Y. Espinaco, S.E. Zorrilla, G.A. Sihufe, Astaxanthin production by autotrophic cultivation of *Haematococcus pluvialis*: a success story. Global Perspectives on Astaxanthin, Elsevier, 2021, pp. 71–89, https://doi.org/10.1016/B978-0-12-823304-7.00005-2.

[10] M. Hayashi, T. Ishibashi, D. Kuwahara, K. Hirasawa, Commercial Production of Astaxanthin with *Paracoccus carotinifaciens*, in: 2021: pp. 11–20. https://doi.org/10.1007/978-981-15-7360-6_2.

[11] C.U. Mussagy, J.F.B. Pereira, L. Dufossé, Astaxanthin production using *Paracoccus carotinifaciens*: a way forward? Trends Biotechnol. (2023) https://doi.org/10.1016/j.tibtech.2023.01.016.

[12] T. Ide, M. Hoya, T. Tanaka, S. Harayama, Enhanced production of astaxanthin in *Paracoccus* sp. strain N-81106 by using random mutagenesis and genetic engineering, Biochem. Eng. J. 65 (2012) 37–43, https://doi.org/10.1016/j.bej.2012.03.015.

[13] C.U. Mussagy, A. Kot, L. Dufossé, C.N.D.P. Gonçalves, J.F.B. Pereira, V.C. Santos-Ebinuma, V. Raghavan, A. Pessoa, Microbial astaxanthin: from bioprocessing to the market recognition, Appl. Microbiol. Biotechnol. 107 (2023) 4199–4215, https://doi.org/10.1007/s00253-023-12586-1.

[14] A. Bassijeh, S. Ansari, S.M.H. Hosseini, Astaxanthin encapsulation in multilayer emulsions stabilized by complex coacervates of whey protein isolate and Persian gum and its use as a natural colorant in a model beverage, Food Res. Int. 137 (2020) 109689, https://doi.org/10.1016/j.foodres.2020.109689.

[15] W. Sun, L. Qiao, X. Li, J. Gu, Y. Zhou, P. Wang, The relationship between the surface color and astaxanthin concentration of different fillet parts of Atlantic salmon under mariculture and freshwater farming modes, J. Food Compos. Anal. 123 (2023) 105506, https://doi.org/10.1016/j.jfca.2023.105506.

[16] C. Liu, B. Hu, Y. Cheng, Y. Guo, W. Yao, H. Qian, Carotenoids from fungi and microalgae: a review on their recent production, extraction, and developments, Bioresour. Technol. 337 (2021) 125398, https://doi.org/10.1016/j.biortech.2021.125398.

[17] Z.T. Harith, D. Charalampopoulos, A. Chatzifragkou, Rapeseed meal hydrolysate as substrate for microbial astaxanthin production, Biochem. Eng. J. 151 (2019) 107330, https://doi.org/10.1016/j.bej.2019.107330.

[18] A.R. Domínguez-Bocanegra, T. Ponce-Noyola, J.A. Torres-Muñoz, Astaxanthin production by *Phaffia rhodozyma* and *Haematococcus pluvialis*: a comparative study, Appl. Microbiol. Biotechnol. 75 (2007) 783–791, https://doi.org/10.1007/s00253-007-0889-9.

[19] T. Zhao, X. Yan, L. Sun, T. Yang, X. Hu, Z. He, F. Liu, X. Liu, Research progress on extraction, biological activities and delivery systems of natural astaxanthin, Trends Food Sci. Technol. 91 (2019) 354–361, https://doi.org/10.1016/j.tifs.2019.07.014.

[20] FDA, Substances Added to Food (formerly EAFUS), Https://Hfpappexternal.Fda.Gov/Scripts/Fdcc/Index.Cfm?Set=FoodSubstances&id=MENTHOL (2025).

[21] R. Vardanega, P. Cerezal-Mezquita, P.C. Veggi, Supercritical fluid extraction of astaxanthin-rich extracts from *Haematococcus pluvialis*: economic assessment, Bioresour. Technol. 361 (2022) 127706, https://doi.org/10.1016/j.biortech.2022.127706.

[22] G. Sanzo, S. Mehariya, M. Martino, V. Larocca, P. Casella, S. Chianese, D. Musmarra, R. Balducchi, A. Molino, Supercritical carbon dioxide extraction of astaxanthin, lutein, and fatty acids from *Haematococcus pluvialis* microalgae, Mar. Drugs 16 (2018) 334, https://doi.org/10.3390/md16090334.

[23] P. Thana, S. Machmudah, M. Goto, M. Sasaki, P. Pavasant, A. Shotipruk, Response surface methodology to supercritical carbon dioxide extraction of astaxanthin from *Haematococcus pluvialis*, Bioresour. Technol. 99 (2008) 3110–3115, https://doi.org/10.1016/j.biortech.2007.05.062.

[24] T.-B. Zou, Q. Jia, H.-W. Li, C.-X. Wang, H.-F. Wu, Response surface methodology for ultrasound-assisted extraction of astaxanthin from *Haematococcus pluvialis*, Mar. Drugs 11 (2013) 1644–1655, https://doi.org/10.3390/md11051644.

[25] K.S. Khoo, K.W. Chew, G.Y. Yew, S. Manickam, C.W. Ooi, P.L. Show, Integrated ultrasound-assisted liquid biphasic flotation for efficient extraction of astaxanthin from *Haematococcus pluvialis*, Ultrason. Sonochem. 67 (2020) 105052, https://doi.org/10.1016/j.ultsonch.2020.105052.

[26] K.S. Khoo, K.W. Chew, G.Y. Yew, S. Manickam, C.W. Ooi, P.L. Show, Integrated ultrasound-assisted liquid biphasic flotation for efficient extraction of astaxanthin from *Haematococcus pluvialis*, Ultrason. Sonochem. 67 (2020) 105052, https://doi.org/10.1016/j.ultsonch.2020.105052.

[27] C.U. Mussagy, A.V. Caicedo Paz, P. Cornejo, C. Santander, F. González, R. G. Voloua, X. Besoain, A. Larach, A. Salinas, K. Godoy, D. Sangaré, CFD insights into microwave- assisted deep eutectic solvent for the recovery of astaxanthin from bacteria *Paracoccus carotinifaciens*: from extraction to agricultural applications, Sep. Purif. Technol. 360 (2025) 131212, https://doi.org/10.1016/j.seppur.2024.131212.

[28] Y. Fan, Z. Niu, C. Xu, L. Yang, F. Chen, H. Zhang, Biocompatible protic ionic liquids-based microwave-assisted liquid-solid extraction of astaxanthin from *Haematococcus pluvialis*, Ind. Crops Prod. 141 (2019) 111809, https://doi.org/10.1016/j.indcrop.2019.111809.

[29] R. Kapoore, T. Butler, J. Pandhal, S. Vaidyanathan, Microwave-assisted extraction for microalgae: from biofuels to biorefinery, Biology 7 (2018) 18, https://doi.org/10.3390/biology7010018.

[30] D.L. Nonglait, J.S. Gokhale, Review insights on the demand for natural pigments and their recovery by emerging microwave-assisted extraction (MAE), Food Bioproc. Tech. 17 (2024) 1681–1705, https://doi.org/10.1007/s11947-023-03192-0.

[31] S. Chen, S. Cen, R. Liu, C. Tao, S. Guo, G. Chen, Microwave reactor with combined rigid and flexible stirring paddles for improving fluid heating uniformity in soft manganese ore leaching processes, ACS Omega 8 (2023) 42367–42378, https://doi.org/10.1021/acsomega.3c04679.

[32] A. Vanessa Caicedo Paz, F. Rigano, C. Cafarella, A. Tropea, L. Mondello, J. Paul Martinez Galan, M. Ahmad, A. Mustafa, F. Farias, A. Córdova, D. Giuffrida, L. Dufossé, C. Ussemane Mussagy, Process intensification of ultrasound assisted deep eutectic solvent-based extraction of astaxanthin-rich extract derived from the non-conventional bacterium *Paracoccus carotinifaciens*, Sep. Purif. Technol. 339 (2024) 126674, https://doi.org/10.1016/j.seppur.2024.126674.

[33] E.D. Revellame, D.L. Fortela, W. Sharp, R. Hernandez, M.E. Zappi, Adsorption kinetic modeling using pseudo-first order and pseudo-second order rate laws: a review, Clean. Eng. Technol. 1 (2020) 100032, https://doi.org/10.1016/j.clet.2020.100032.

[34] M.C. Dal, N. Onursal, Two new linearized equations derived from the pseudo-second-order kinetic model, Desalin. Water Treat. 308 (2023) 183–189, https://doi.org/10.5004/dwt.2023.29992.

[35] T. Belwal, F. Chemat, P.R. Venskutonis, G. Cravotto, D.K. Jaiswal, I.D. Bhatt, H. P. Devkota, Z. Luo, Recent advances in scaling-up of non-conventional extraction techniques: learning from successes and failures, TrAC. Trends Anal. Chem. 127 (2020) 115895, https://doi.org/10.1016/j.trac.2020.115895.

[36] R. Sinnott, G. Towler, Costing and project evaluation. Chemical Engineering Design, Elsevier, 2020, pp. 275–369, https://doi.org/10.1016/B978-0-08-102599-4.00006-0.

[37] S. Aprile, V. Venturi, F. Presini, A. Mustafa, M.S. Sadek, A. Inayat, D. Remonatto, P. P. Giovannini, L.A. Lerin, Techno-economic assessment of benzyl benzoate clean production using conventional heating or microwaves, Sustain. Chem. Pharm. 36 (2023) 101257, https://doi.org/10.1016/j.scp.2023.101257.

[38] N.Sh El-Gendy, M. Shaaban Sadek, H.N. Nassar, A. Mustafa, Eco-friendly extraction of sustainable and valorized value-added products from *Ulva fasciata* Macroalgae: a holistic technoeconomic analysis, Int. J. Biomater. 2025 (2025), https://doi.org/10.1155/ijbm/5811057.

[39] A.V. Bridgwater, C.J. Mumford, Waste recycling and pollution control handbook, Godwin, London, 1979.

[40] C.U. Mussagy, A.C.R.V. Dias, V.C. Santos-Ebinuma, M. Shaaban Sadek, M. Ahmad, C.R. de Andrade, F.F. Haddad, J.L. dos Santos, C.B. Scarim, J.F.B. Pereira, J.

F. Floriano, R.D. Herculano, A. Mustafa, Is the carotenoid production from *Phaffia rhodozyma* yeast genuinely sustainable? a comprehensive analysis of biocompatibility, environmental assessment, and techno-economic constraints, Bioresour. Technol. 397 (2024) 130456, https://doi.org/10.1016/j.biortech.2024.130456.

[41] C.U. Mussagy, N.F. Ramos, A.V. Caicedo-Paz, F.O. Farias, A. Luísa R. Gini, C. B. Scarim, P. E. L. L. Filho, R.D. Herculano, M. Shaaban Sadek, M. Ahmad, A. Mustafa, L. Dufossé, Techno-economic insights into one-pot bacterial astaxanthin extraction and sustainable therapeutic product development using natural solvent mixtures, Sep. Purif. Technol. 356 (2025) 129926, https://doi.org/10.1016/j.seppur.2024.129926.

[42] Economics, United States Federal Corporate Tax Rate, Https://Tradingeconomics.Com/United-States/Corporate-Tax-Rate (2025).

[43] A. Sridhar, M. Ponnuchamy, P.S. Kumar, A. Kapoor, D.-V.N. Vo, S. Prabhakar, Techniques and modeling of polyphenol extraction from food: a review, Environ. Chem. Lett. 19 (2021) 3409–3443, https://doi.org/10.1007/s10311-021-01217-8.

[44] B. Yang, X. Fan, D. Li, L. Cui, C. Chang, L. Yan, B. Lu, J. Li, Simulation and experimental study of solid–liquid extraction of coal tar residue based on different extractants, ACS Omega 8 (2023) 47835–47845, https://doi.org/10.1021/acsomega.3c06290.

[45] P. Hobbi, O.V. Okoro, C. Delporte, H. Alimoradi, D. Podstawczyk, L. Nie, K. V. Bernaerts, A. Shavandi, Kinetic modelling of the solid–liquid extraction process of polyphenolic compounds from apple pomace: influence of solvent composition and temperature, Bioresour. Bioprocess. 8 (2021) 114, https://doi.org/10.1186/s40643-021-00465-4.

[46] S. Fraterrigo Garofalo, F. Demichelis, V. Peletti, L. Picco, T. Tommasi, D. Fino, Comparative study of polyphenol extraction using physical techniques and water as a solvent: a sustainable approach for the valorization of apple pomace, Environ. Sci. Pollut. Res. (2024), https://doi.org/10.1007/s11356-024-34637-4.

[47] C.U. Mussagy, N.F. Ramos, A.V. Caicedo P, F.O. Farias, M. Ahmad, A. Mustafa, V. Raghavan, Tuning bio-derived solvents for the rapid solubilization of astaxanthin-rich extracts from non-conventional bacterium *Paracoccus carotinifaciens*, Sep. Purif. Technol. 346 (2024) 127542, https://doi.org/10.1016/j.seppur.2024.127542.

[48] B. Liu, M. Finkel, P. Grathwohl, First order approximation for coupled film and intraparticle pore diffusion to model sorption/desorption batch experiments, J. Hazard. Mater. 429 (2022) 128314, https://doi.org/10.1016/j.jhazmat.2022.128314.

[49] G.G. López, M.M. Brousse, A.R. Linares, Kinetic modelling of total phenolic compounds from *Ilex paraguariensis* (St. Hil.) leaves: conventional and ultrasound assisted extraction, Food Bioprod. Process. 139 (2023) 75–88, https://doi.org/10.1016/j.fbp.2023.03.003.

[50] J. Queffelec, W. Beraud, S. Ferron, J. Boustie, I. Rodríguez-González, B. Díaz-Reinoso, M.D. Torres, H. Domínguez, Alternatives for the extraction of bioactives and biopolymers from *Evernia prunastri* for the formulation of antimicrobial bio-based films, Green. Chem. 26 (2024) 10205–10224, https://doi.org/10.1039/D4GC02741H.